www.MaterialsViews.com

Ion Beam Sputtering Deposition

Controlled Growth of Few-Layer Hexagonal Boron Nitride on Copper Foils Using Ion Beam Sputtering Deposition

Haolin Wang, Xingwang Zhang, Junhua Meng, Zhigang Yin, Xin Liu, Yajuan Zhao, and Liuqi Zhang*

Two-dimensional (2D) atomic crystals have recently received a great deal of attention due to their unique structure, many fascinating properties and a wide range of technological applications.[1–3] Hexagonal boron nitride (h-BN), a 2D insulator with a wide band gap (5~6 eV), has the same atomic structure as graphene, consisting of sp^2-bonded alternating boron and nitrogen atoms in a honeycomb arrangement within each layer.[4–6] The small lattice mismatch (1.7%) with graphene, along with its atomically smooth surface that is relatively free of dangling bonds and trapped charges, makes h-BN a suitable substrate for graphene electronics. Indeed, the mobility for graphene devices on h-BN was observed to be an order of magnitude higher than that of the devices fabricated on commonly used SiO_2/Si substrate.[7,8] Furthermore, h-BN possesses low dielectric constant and high breakdown field, thus raising its potential as a high-quality gate dielectric layer.[9–11]

Similar to graphene, h-BN flakes can be produced by mechanical or liquid-phase exfoliation, nevertheless, the limited flake size hinders their applications in large area devices.[3,4] Monolayer and few-layer h-BN have been grown on single-crystal transition metals such as Ru (001), Rh (111), and Pt (111) with expensive ultrahigh vacuum (UHV) systems by chemical vapor deposition (CVD) from borazine[12–14] or magnetron sputtering of B target in Ar/N_2,[15] respectively. However, it is rather difficult to controllably grow h-BN and to transfer it onto other substrates, due to the complex nature of the UHV systems used. Recently, both atmospheric pressure CVD and low-pressure CVD have also been used to grow monolayer and few-layer h-BN on Cu,[16–20] Ni,[21,22] and Pt substrates.[23,24] A common practical problem during the CVD process is the need to utilize some unconventional precursors, such as powdered ammonia borane (H_3B-NH_3),[16–20,23–25] liquid borazine ($B_3N_3H_6$),[9,12–14,21] and gaseous diborane/ammonia (B_2H_6/NH_3).[22] These compounds are not only very expensive, but also highly toxic, unstable, or pyrophoric in nature.[26] Furthermore, the synthesis of h-BN by CVD is relatively complicated since the growth parameters governing CVD processes are closely interrelated. As a result, the elaborated process parameters are typically required, and otherwise the growth results are not easy to control or reproduce.[26] Therefore, it is highly desirable to develop a facile and efficient method for producing high-quality large area 2D h-BN films to further exploit their properties and potential applications.

In this work, we demonstrate a facile and innovative method of growing high quality few-layer h-BN by ion beam sputtering deposition (IBSD). By sputtering a benign and nontoxic h-BN target with an Ar ion beam, both triangle and polygonal h-BN domains were achieved on Cu foils. The domain density of h-BN can be reduced by introducing H_2 into the deposition chamber, resulting in an increased size of h-BN domains. The possible mechanisms of h-BN growth were also described and discussed. Compared to CVD, IBSD growth avoids the use of unconventional precursors and it is also much easier to control, which should be very useful for the large-scale production of h-BN.

The growth of h-BN layers was carried out at 1050 °C in an IBSD system with a Kaufmann ion source. Compared to magnetron sputtering, one benefit of IBSD is that the Ar plasma is restricted in the ion source, eliminating the side effect of plasma in the sputtering process. For the growth process, a cleaned Cu foil was firstly annealed at 1050 °C for 20 min under 20 sccm (standard cubic centimeters per minute) H_2 atmosphere. Then, boron and nitrogen species were sputtered from a pure h-BN target by a 1.0-keV Ar ion beam, resulting in the growth of 2D h-BN on the Cu foil. To study the effect of the ambient conditions, H_2 was introduced into the growth chamber during sputtering. After growth, the h-BN films on Cu foils were cooled down to room temperature in Ar atmosphere quickly and then transferred onto different substrates for characterization. The growth protocol is illustrated in Figure S1.

Figure 1a shows a typical scanning electron microscopy (SEM) image of h-BN domains grown at 1050 °C on Cu foil for 4 min in pure Ar with a flow rate of 4 sccm. Besides commonly reported triangular domains,[18,20,22,27] most h-BN domains exhibit asymmetrical hexagonal or irregular polygonal shape, and the white particles were frequently observed on the center of h-BN domains. As shown in the inset of Figure 1a, most of the white particles show a triangular pyramid shape, which are the multilayer h-BN stacks, indicating

H. L. Wang, Prof. X. W. Zhang, J. H. Meng, Dr. Z. G. Yin, X. Liu, Y. J. Zhao, L. Q. Zhang
Key Lab of Semiconductor Materials Science
Institute of Semiconductors
Chinese Academy of Sciences
Beijing 100083, P. R. China
E-mail: xwzhang@semi.ac.cn

DOI: 10.1002/smll.201402468

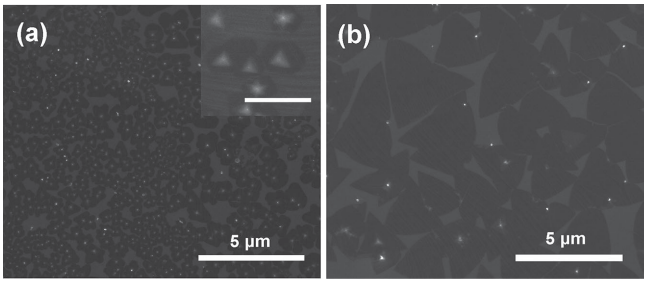

Figure 1. SEM images of h-BN domains deposited on the Cu foils at 1050 °C for 4 min under (a) pure Ar and (b) Ar/H_2 mixed atmosphere. The inset in (a) reveals that the triangular white particles are the multilayer h-BN stacks, and the scale in the inset is 1 μm.

the growth of h-BN by IBSD is not self-limited. It can be seen that the domain density is high and the size of h-BN domains ranges approximately from 0.2 to 1 μm. In addition, the growth of h-BN was influenced by annealing of the Cu foil in H_2 atmosphere. For the sample without pre-annealing of Cu foil, the h-BN domains appeared to be very small and tended to coalesce, and a large number of the impurity particles were observed on Cu surface (Figure S2).

In general, as the domains coalesce to form a continuous film, large-sized domains will lead to a low density of grain boundaries and defects, resulting in a higher quality of film for electronic device applications. Reducing domain density is a common approach to obtain large-sized crystalline domains.[19,20] It was reported that high-temperature exposure to pure H_2 can etch the existing h-BN domains.[14] Therefore, we expect that the domain density will be reduced by introducing H_2 into the deposition chamber, enabling the growth of larger-sized h-BN domains during the extended growth time. Along this line, h-BN domains were synthesized by introducing 3 sccm H_2 into the deposition chamber during sputtering. Figure 1b shows an SEM image of h-BN domains formed on Cu foils under the same growth conditions with the addition of H_2. It is clear that the triangular h-BN domains were observed to be dominant under Ar/H_2 atmosphere, which are randomly oriented even within the same Cu grain apart from a few exception (Figure S3a), indicating a weak interaction at h-BN/Cu interface. More importantly, the density of h-BN domains is significantly reduced and the size of the triangular domain (5 μm) is 4~5 times larger than that of the sample without H_2. Furthermore, most of the white particles (multilayer h-BN stacks) on top of h-BN domains disappeared after introducing H_2, and the second layer of triangular h-BN domain was only occasionally observed. Obviously, the addition of H_2 is really able to inhibit the growth of h-BN, leading to the formation of large-sized h-BN domains. It can also be seen that individual h-BN domains can grow across Cu grain boundaries (Figure S3b), and the nucleation sites are evenly distributed on the Cu surface. These results suggest that the Cu grains have little influence on the shape and density of the h-BN domains, which is different from the preferential nucleation near or on the Cu grain boundaries during the CVD growth of h-BN.[18,19]

Transmission electron microscopy (TEM) was utilized to characterize the structure of grown h-BN domains. **Figure 2**a shows a representative high-resolution TEM (HRTEM) image recorded at an h-BN domain transferred onto TEM grids. Lattice fringes revealed the h-BN (100) lattice plane with d spacing of 0.24 nm, which is in good agreement with earlier published values.[20–22] The selective area electron diffraction (SAED) pattern, as shown in the inset of Figure 2a, clearly shows a set of hexagonal diffraction spots matched well with the (10–10) index of h-BN. These TEM characterizations reveal the single crystal nature of the examined areas, suggesting the high quality of the grown h-BN domains. In some regions the edges of h-BN domains are suspended across the TEM grid openings, allowing for a cross sectional view of the film. Both bilayer and few-layer h-BN were observed from the TEM images, as shown in Figure S4, The average interlayer distance of the h-BN is nearly 0.35 nm, consistent with the reported value for the h-BN structure.[17,21] Figure 2b shows a typical atomic force microscopy (AFM) image of the h-BN domains transferred onto a SiO_2/Si substrate, and sharp edges of the h-BN domains can be observed clearly. From the height profile of the AFM image, the thickness of the h-BN domain is estimated to be about 0.7 nm, consistent with bilayer growth. Besides h-BN bilayer, few-layer h-BN flakes with thicknesses of 1.7~2.4 nm can also be recognized in the AFM height image, as shown in Figure 2c.

Figure 2d shows a typical Raman spectrum taken from the h-BN domain transferred onto a SiO_2/Si substrate. A characteristic Raman peak of h-BN was observed at about 1371 cm^{-1}, corresponding to the E_{2g} vibrational mode within a h-BN layer.[28,29] To investigate the optical properties of h-BN, UV-visible spectroscopy was performed on the h-BN layer transferred onto a quartz substrate. As shown in Figure 2e, almost zero absorbance was detected in the visible-light range, and a strong absorption peak at 202 nm was observed in the UV region, indicating the presence of an optical bandgap. As a direct-gap semiconductor, the optical bandgap of h-BN layer can be extracted from the UV-visible spectra by using the following relationship: $\alpha E = C(E-E_g)^{1/2}$, where α is the absorption coefficient, C is a constant, E is the incident photo energy, and E_g is the optical bandgap energy.[30] As displayed in the inset of Figure 2e, the optical bandgap of 5.92 eV was calculated from the X axis intercept of the linear part of the plot $(\alpha E)^2$ *vs* E, which is consistent with the previously reported values.[21,23,31]

X-ray photoelectron spectroscopy (XPS) and near-edge X-ray absorption fine structure (NEXAFS) were also applied to characterize the elemental stoichiometry and electronic structure of the as-grown h-BN domains on Cu foils. The binding energies of B 1s and N 1s are located at 190.5 and 398.1 eV, respectively, as shown in Figure 2f,g. These values are in good agreement with the previously reported values in both h-BN bulk and ultrathin films.[19–22] The B/N ratio from our XPS survey was calculated to be 0.97, which is very close to the 1:1 stoichiometry of h-BN. In addition, Figure 2f also exhibits a broad satellite peak at about 8.0 eV higher binding energy than the B 1s core level peak. It has been reported that there is a π plasmon loss feature at about 9 eV higher binding energy and a satellite peak associated with the π–π^* transition in the sp^2 bonded h-BN at about 6.2~6.5 eV higher binding energy.[32] Hence, the satellite peak of B1s

www.MaterialsViews.com

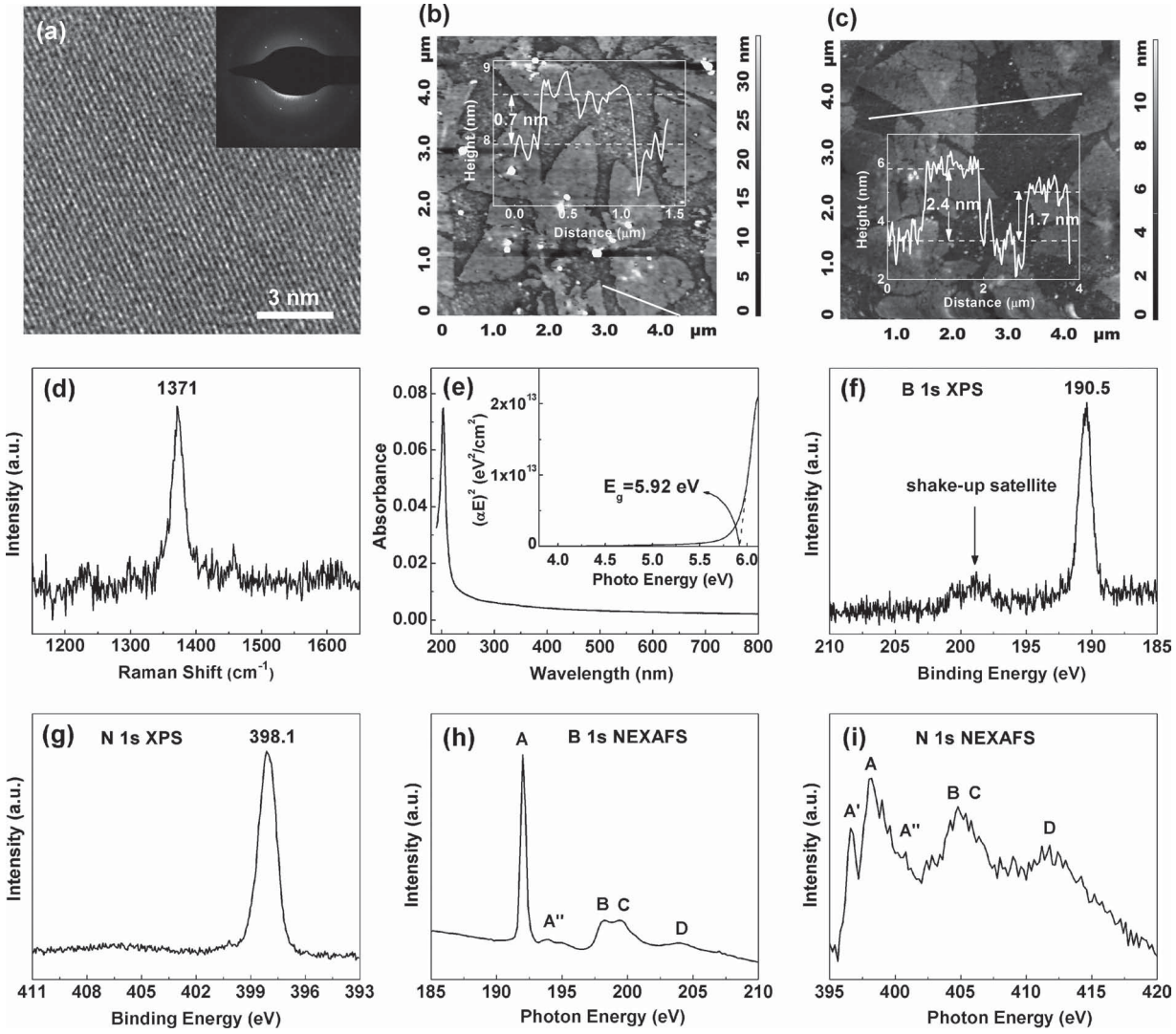

Figure 2. Characterization of h-BN domains. (a) top view HRTEM image and the corresponding SAED pattern (inset) of h-BN domains showing features of a hexagonal lattice. (b, c) AFM images of h-BN domains transferred onto a SiO_2/Si substrate, and the height profiles along the white lines drawn in the AFM images show thicknesses of 0.7 nm and 1.7–2.4 nm, respectively. (d) Raman spectrum of h-BN domains on a Si/SiO_2 substrate. (e) UV-Vis spectrum of h-BN film transferred on a transparent quartz substrate. The inset shows optical bandgap (5.92 eV) analysis of h-BN from (e). XPS spectra of (f) B 1s and (g) N 1s, (h, i) NEXAFS spectra of B 1s and N 1s, respectively. All NEXAFS spectra were recorded with an angle of incidence of 90°.

at about 198.5 eV can be considered as a combined peak of the two features of h-BN. The B 1s and N 1s NEXAFS spectra from the h-BN domains grown on Cu foils are shown in Figure 2h,i, respectively, which are similar to the reported results of the monolayer h-BN chemisorbed on Cu (111).[33] All spectral features for both B 1s and N 1s NEXAFS can be divided into two groups: features labeled A, A′ and A″ reflect transitions of a core electron into the states of π symmetry, while all the remaining features correspond to transitions with predominantly in-plane σ character.[33] These results reveal that the configuration of B and N atoms in the sample is the sp^2 hybridized B-N bond, implying the existence of the hexagonal phase in our BN domains.

To understand the nucleation and growth mechanism, we investigated the growth of h-BN from 600 °C up to 1050 °C for different time periods. Here, the maximum temperature (1050 °C) was chosen close to the Cu melting point (1084 °C). **Figure 3**a-d shows the SEM images of the h-BN domains prepared at 1050, 950, 850, and 750 °C for 4 min with the addition of 3 sccm H_2, respectively. Noticeably, the lower substrate temperature resulted in a significant decrease in the average domain size and a slightly increased coverage rate of h-BN domains, as well as irregular shapes instead of the usual triangles at 1050 °C. The average size of h-BN domains changed approximately from 3 μm to 1 and 0.5 μm when the growth temperature was reduced from 1050 °C to 950 and 850 °C, respectively. As the growth temperature was decreased to 750 °C, the h-BN domains were so densely that they covered almost the whole Cu surface, as shown in Figure 3d. When the temperature further decreased to 600 °C, the domain structure could not be distinguished anymore and a homogeneous BN film was formed on the

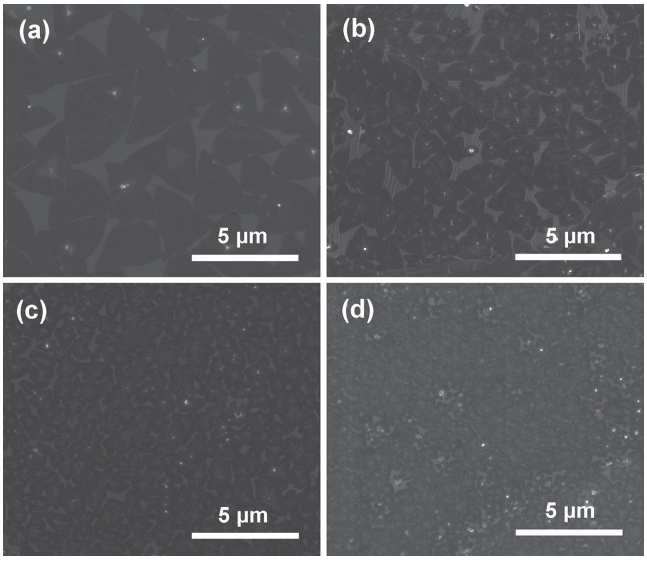

Figure 3. SEM images of the h-BN domains prepared on the Cu foils at (a) 1050, (b) 950, (c) 850, and (d) 750 °C for 4 min with the addition of 3 sccm H_2.

substrate surface (Figure S5a). However, in this case, the characteristic Raman peak of h-BN at around 1371 cm^{-1} is completely missing, as shown in Figure S5b, implying only an amorphous phase was obtained at 600 °C.

Next we show the time dependent evolution of h-BN domains prepared by IBSD on Cu foils. **Figure 4**a-d shows the SEM images of h-BN prepared at 1050 °C under 1, 2, 4, 10 min of growth time, respectively. During the initial stage of h-BN growth, besides characteristic triangles, many abnormal structures composed of intersecting or joining triangles were imaged as butterfly-like and star-like structures (Figure 4a,b), which is similar to the case of CVD MoS_2 and WS_2.[34] For

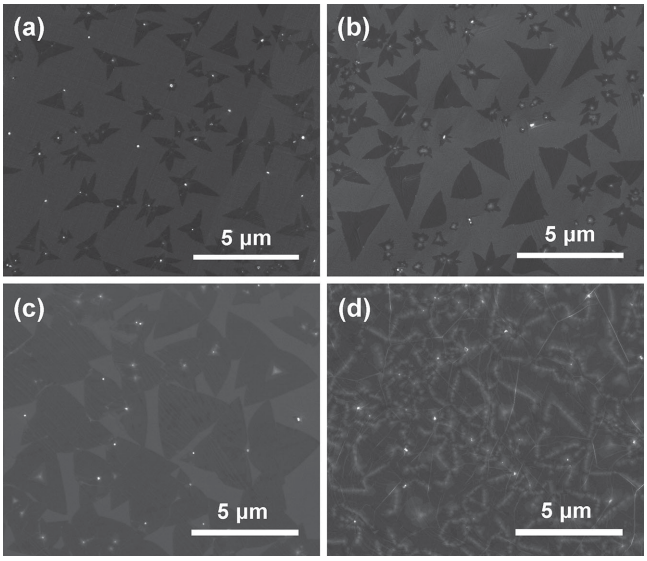

Figure 4. The time dependent evolution of h-BN domains prepared by IBSD on the Cu foils. SEM images of h-BN domains prepared at 1050 °C under (a) 1, (b) 2, (c) 4, and (d) 10 min of growth time.

4 min growth, nearly all the h-BN domains are in triangular shapes. Further increasing the growth time to 10 min, the growing h-BN domains might contact with the adjacent domains and merge into a continuous film as shown in Figure 4d. Apart from the h-BN grain boundaries, the overall contrast of the h-BN film is uniform. It can be seen from Figure 4 that the size of h-BN domains is increased while its density almost keeps a constant with increasing growth times. This is quite different from the case of CVD growth process, in which the initial h-BN domains were increased both in size and density for longer growth times.[18]

The above results indicate that the irregular polygonal h-BN domains with the size less than 1 μm were formed in pure Ar atmosphere, while the addition of H_2 to the deposition chamber led to the growth of triangular h-BN domains with the size of 5 μm. Although an exact mechanism of the formation of h-BN domains is not known, a possible explanation is as follows. B and N atoms are sputtered from the h-BN target by the Ar ion beam. They diffuse and agglomerate to form BN clusters, which then diffuse and collide with each other, forming the initial h-BN nuclei. After nucleation of h-BN, it grows by surface attachment of B and N atoms as well as BN radicals and forms an h-BN domain. The most important surface processes (**Figure 5**a) involved in h-BN formation under pure Ar atmosphere are adsorption of sputtered species (AD), desorption of species (DE), surface diffusion of species (SD), cluster collisions and formation of h-BN nuclei (CFN), as well as attachment of B/N atoms and cluster into the h-BN domains (AAC). The nucleation density of h-BN under pure Ar atmosphere is considerably high, which limits the size of h-BN domains to less than 1 μm. When H_2 is introduced into the deposition chamber, two additional processes, the H-induced etching of h-BN (HE) and edge passivation (EP) by hydrogen, have to be considered. The elementary steps involved in the H etching process are the H-assisted detachment of B and N from the h-BN edge, followed by a desorption of the hydrated BH_x and NH_x (and possibly mixed BNH_x).[14] The etching rate of h-BN depends on the size of h-BN nucleus/domain since the ratio of edge atoms to basal atoms is related closely with the size of nucleus/domain. The smaller nucleus means the higher ratio of edge atoms to basal atoms. As a result, the H etching leads to diminution and even vanishing of the smaller h-BN nuclei, and thus eventually suppression of the h-BN growth. Furthermore, when edge-attachment and lattice integration involves dehydrogenation at domain edges, the edge-attachment barrier is effectively reduced, promoting lateral growth of h-BN domains.[19] With a combination of suppressed vertical growth and enhanced lateral growth rate due to introducing hydrogen, the larger h-BN domains with a size of 5 μm can be obtained.

Besides the deposition atmosphere, the growth temperature also has a significant effect on the shape and coverage of h-BN domains. It is well known that the increasing temperature will lead to more effective desorption of species, causing a dramatic depletion of species required for nucleation/growth. Consequently, with increasing temperature the growth rate of h-BN decreases, which results in the lower surface coverage of h-BN at the higher temperature as seen

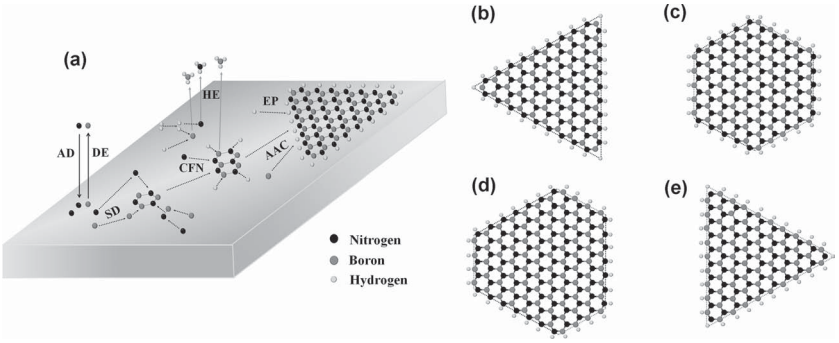

Figure 5. (a) Schematic view of mechanisms involved in the nucleation and growth of 2D h-BN on Cu foils by IBSD. Schematic illustration of atoms arrangement of h-BN domains with different shapes: (b) the triangle with N-terminated edges, (c) the regular hexagon with alternating B- and N-terminated edges, (d) the irrigular hexagon with alternating B and N-terminated edges, and (e) the triangle with B-terminated edges. A theoretical modeling on growth of h-BN suggests that the equilibrium shapes of h-BN is dependent on the chemical potential μ.

in Figure 3. On the other hand, the increasing temperature will also enhance surface diffusion of species and effectively reduce the edge-attachment barrier, enabling them to have longer diffusion length and move freely along the active edges. Both of them are favorable for the lateral growth of h-BN domains, thus producing larger h-BN domains as shown in Figure 3a.

Regarding the shape of h-BN domains, a recent theoretical modeling[35] on growth of h-BN suggests that, unlike in the case of mono-elemental graphene, the shapes of h-BN can vary broadly with the chemical potential μ as shown in Figure 5b-e. They found that triangular shape h-BN domains with all three sides with N-termination are dominant under H atmosphere because the N-terminated zigzag edges (Figure 5b) have lower edge energy than that of B-terminated ones (Figure 5e).[35] This is also the reason why our h-BN domains prepared with Ar/H_2 atmosphere at higher temperature (1050 °C) are triangular in shape. Actually, besides a few exceptions,[18,19] the h-BN domains prepared using CVD method tended to nucleate in triangular shape on various metallic surfaces.[18,20,22,27] However, the absence of H during the growth of h-BN or the decreasing temperature will lead to the change of chemical potential μ. We propose that in this case the N-terminated and B-terminated edges have similar edge energies, and as a result, the irregular polygonal h-BN domains were formed due to the competition between different shapes.

In conclusion, we have successfully synthesized 2D h-BN domains with a size up to 5 μm on Cu foils using IBSD. It was found that the smaller irregular polygonal h-BN domains were formed in pure Ar atmosphere, while the larger triangular domains were obtained by introducing H_2 into the deposition chamber due to the suppressed vertical growth and enhanced lateral growth rate. Besides the deposition atmosphere, the growth temperature has a significant effect on the shape and coverage of h-BN domains. This facile and innovative growth method is highly reproducible with a large margin of process conditions. Compared to the conventional CVD method, the IBSD technique avoids the use of unconventional precursors and is much easier to control, which should be very useful for the large-scale production of 2D h-BN layers. In addition, unlike CVD, it is possible to exploit this approach to directly grow h-BN on other substrates such as SiO_2/Si.

Experimental Section

Growth of h-BN by IBSD: The growth of h-BN layers was carried out on the Cu foils in an IBSD chamber equipped with a Kaufmann ion source. Prior to the growth, the Cu foil (99.8% purity, 25 μm thickness, Alfa Asear) was washed by diluted nitric acid (5%) and deionized (DI) water for a few seconds to remove the surface oxidized layer and then loaded into the sample holder. The chamber was firstly pumped to the base pressure (2×10^{-5} Pa), and then the Cu foil was annealed at 1050 °C for 20 min under 20 sccm H_2 atmosphere to obtain a clean and smooth surface. After annealing of Cu, the chamber was again pumped to the base pressure, and then Ar gas (4 sccm) was introduced into ion source and 3 sccm H_2 was filled with the chamber. A pure h-BN target (99.0% purity, Good Fellow) was sputter eroded using the Ar^+ ion beam (1.0 keV, 0.3 mA·cm^{-2}). During the sputtering process, the chamber was kept at a constant pressure (3×10^{-2} Pa). After the growth procedure, the ion source was shut down and the sample was cooled down to room temperature in pure Ar atmosphere quickly.

Transfer: The as-grown h-BN was transferred on to different substrates for characterization with the same method for graphene. Polymethyl methacrylate (PMMA) (4.0% in anisole) was spun on the as-grown h-BN on Cu with 2500 rpm for 1 min, and then the underlying Cu was etched away by Marble reagent. Next, the PMMA/h-BN film was washed by DI water to remove the residual reagent. After that the h-BN could be transferred to the target substrates. At last, PMMA layers were dissolved in acetone, and the well-prepared h-BN was obtained for subsequent characterization.

Characterization: The morphology and structure of h-BN layers were characterized using SEM (FEI Quanta-600), AFM (NTMDT Solver P47, tapping mode), and TEM (Tecnai F30, 300 kV). Raman spectroscopy was measured with a Renishaw inVia-Reflex spectrometer using a 532 nm laser as the excitation source. Optical absorption spectra of the samples were acquired by using a Varian Cary 5000 UV-Vis spectrophotometer in a double-beam mode. X-ray photoelectron spectroscopy (XPS) measurements were performed on an EscaLab 250Xi instrument with a monochromated Al Kα source (1486.68 eV). Near-edge X-ray absorption fine structure (NEXAFS) measurements were carried out using synchrotron radiation at beam line 4B9B of Beijing Synchrotron Radiation Facility (BSRF).

Supporting Information

Supporting Information is available from the Wiley Online Library or from the author.

Acknowledgements

This work was financially supported by the National Basic Research Program of China (No. 2012CB619306, 2012CB934200), the National Natural Science Foundation of China (No. 61376007) and the Beijing Natural Science Foundation (No. 2142032). We are thankful to Dr. X. M. Meng and Mr. J. Xia of the Technical Institute of Physics and Chemistry, CAS for the cross-sectional TEM measurements.

[1] K. S. Novoselov, A. H. Castro Neto, *Phys. Scr.* **2012**, *T146*, 014006.
[2] S. Z. Butler, S. M. Hollen, L. Cao, Y. Cui, J. A. Gupta, H. R. Gutiérrez, T. F. Heinz, S. S. Hong, J. Huang, A. F. Ismach, E. Johnston-Halperin, M. Kuno, V. V. Plashnitsa, R. D. Robinson, R. S. Ruoff, S. Salahuddin, J. Shan, L. Shi, M. G. Spencer, M. Terrones, W. Windl, J. E. Goldberger, *ACS Nano* **2013**, *7*, 2898.
[3] M. S. Xu, T. Liang, M. M. Shi, H. Z. Chen, *Chem. Rev.* **2013**, *113*, 3766.
[4] D. Pacilé, J. C. Meyer, Ç. Ö. Girit, A. Zettl, *Appl. Phys. Lett.* **2008**, *92*, 133107.
[5] D. Golberg, Y. Bando, Y. Huang, T. Terao, M. Mitome, C. Tang, C. Zhi, *ACS Nano* **2010**, *4*, 2979.
[6] C. G. Lee, Q. Li, W. Kalb, X. Liu, H. Berger, R. W. Carpick, J. Hone, *Science* **2010**, *328*, 76.
[7] C. R. Dean, A. F. Young, I. Meric, C. Lee, L. Wang, S. Sorgenfrei, K. Watanabe, T. Taniguchi, P. Kim, K. L. Shepard, J. Hone, *Nat. Nanotechnol.* **2010**, *5*, 722.
[8] W. Gannett, W. Regan, K. Watanabe, T. Taniguchi, M. F. Crommie, A. Zettl, *Appl. Phys. Lett.* **2011**, *98*, 242105.
[9] K. K. Kim, A. Hsu, X. Jia, S. M. Kim, Y. Shi, M. Hofmann, D. Nezich, J. F. Rodriguez-Nieva, M. Dresselhaus, T. Palacios, J. Kong, *ACS Nano* **2012**, *6*, 8583.
[10] L. Britnell, R. V. Gorbachev, R. Jalil, B. D. Belle, F. Schedin, A. Mishchenko, T. Georgiou, M. I. Katsnelson, L. Eaves, S. V. Morozov, N. M. R. Peres, J. Leist, A. K. Geim, K. S. Novoselov, L. A. Ponomarenko, *Science* **2012**, *335*, 947.
[11] A. M. Goossens, S. C. M. Driessen, T. A. Baart, K. Watanabe, T. Taniguchi, L. M. K. Vandersypen, *Nano Lett.* **2011**, *12*, 4656.
[12] A. Nagashima, N. Tejima, Y. Gamou, T. Kawai, C. Oshima, *Phys. Rev. Lett.* **1995**, *75*, 3918.
[13] M. Corso, W. Auwarter, M. Muntwiler, A. Tamai, T. Greber, J. Osterwalder, *Science* **2004**, *303*, 217.
[14] P. Sutter, J. Lahiri, P. Albrecht, E. Sutter, *ACS Nano* **2011**, *5*, 7303.
[15] P. Sutter, J. Lahiri, P. Zahl, B. Wang, E. Sutter, *Nano Lett.* **2013**, *13*, 276.
[16] L. Song, L. Ci, H. Lu, P. B. Sorokin, C. Jin, J. Ni, A. G. Kvashnin, D. G. Kvashnin, J. Lou, B. I. Yakobson, P. M. Ajayan, *Nano Lett.* **2010**, *10*, 3209.
[17] K. H. Lee, H.-J. Shin, J. Lee, I.-Y. Lee, G.-H. Kim, J.-Y. Choi, S.-W. Kim, *Nano Lett.* **2012**, *12*, 714.
[18] K. K. Kim, A. Hsu, X. Jia, S. M. Kim, Y. Shi, M. Dresselhaus, T. Palacios, J. Kong, *Nano Lett.* **2012**, *12*, 161.
[19] R. Y. Tay, M. H. Griep, G. Mallick, S. H. Tsang, R. S. Singh, T. Tumlin, E. H. T. Teo, S. P. Karna, *Nano Lett.* **2014**, *14*, 839.
[20] L. F. Wang, B. Wu, J. S. Chen, H. T. Liu, P. A. Hu, Y. Q. Liu, *Adv. Mater.* **2014**, *26*, 1559.
[21] Y. Shi, C. Hamsen, X. Jia, K. K. Kim, A. Reina, M. Hofmann, A. L. Hsu, K. Zhang, H. Li, Z.-Y. Juang, M. S. Dresselhaus, L.-J. Li, J. Kong, *Nano Lett.* **2010**, *10*, 4134.
[22] A. Ismach, H. Chou, D. A. Ferrer, Y. Wu, S. McDonnell, H. C. Floresca, A. Covacevich, C. Pope, R. Piner, M. J. Kim, R. M. Wallace, L. Colombo, R. S. Ruoff, *ACS Nano* **2012**, *6*, 6378.
[23] Y. Gao, W. Ren, T. Ma, Z. Liu, Y. Zhang, W.-B. Liu, L.-P. Ma, X. Ma, H.-M. Cheng, *ACS Nano* **2013**, *7*, 5199.
[24] G. Kim, A.-R. Jang, H. Y. Jeong, Z. Lee, D. J. Kang, H. S. Shin, *Nano Lett.* **2013**, *13*, 1834.
[25] L. Liu, J. Park, D. A. Siegel, K. F. McCarty, K. W. Clark, W. Deng, L. Basile, J. C. Idrobo, A.-P. Li, G. Gu, *Science* **2014**, *343*, 163.
[26] X. X. Yang, Z. X. Guan, M. Zeng, J. K. Wei, W. L. Wang, X. D. Bai, *Small* **2013**, *9*, 1353.
[27] N. Guo, J. Wei, L. Fan, Y. Jia, D. Liang, H. Zhu, K. Wang, D. Wu, *Nanotechnology* **2012**, *23*, 415605.
[28] R. Geick, C. H. Perry, G. Rupprecht, *Phys. Rev.* **1966**, *146*, 543.
[29] R. V. Gorvachev, I. Riaz, R. R. Nair, R. Jalil, L. Britnell, B. D. Belle, E. W. Hill, K. S. Novoselov, K. Watanabe, T. Taniguchi, A. K. Geim, P. Blake, *Small* **2011**, *7*, 465.
[30] T. H. Yuzuriha, D. W. Hess, *Thin Solid Films* **1986**, *140*, 199.
[31] K. Watanabe, T. Taniguchi, H. Kanda, *Nat. Mater.* **2004**, *3*, 404.
[32] K. S. Park, D. Y. Lee, K. J. Kim, D. W. Moon, *J. Vac. Sci. Technol. A* **1997**, *12*, 1041.
[33] A. B. Preobrajenski, A. S. Vinogradov, N. Mårtensson, *Surf. Sci.* **2005**, *582*, 21.
[34] A. M. van der Zande, P. Y. Huang, D. A. Chenet, T. C. Berkelbach, Y. You, G.-H. Lee, T. F. Heinz, D. R. Reichman, D. A. Muller, J. C. Hone, *Nat. Mater.* **2013**, *12*, 554.
[35] Y. Liu, S. Bhowmick, B. I. Yakobson, *Nano Lett.* **2011**, *11*, 3113.

Received: August 18, 2014
Revised: September 5, 2014
Published online: November 3, 2014